An Unsupervised Hair Segmentation and Counting System in Microscopy Images

Huang-Chia Shih, *Member, IEEE*

***Abstract*— This paper focuses on the development of medical software for clinical applications using advanced image processing algorithms. Three critical issues of hair segmentation and counting are addressed in this paper. First, the removal of any bright spots due to oil or moisture, which generate circular patterns in the middle of the hair and significantly affect the accuracy of determining the line. Second, two contacting or overlapping hairs are recognized and counted as a single hair. To solve this problem, we proposed a hair-bundling algorithm to calculate any concealed hairs. Finally, hairs may be wavy or curly, making the conventional Hough-based line detection algorithm unsuitable, since it suffers from parameter selections, such as the minimum length of line segment, and distance between line segments. Our proposed hair counting algorithm is substantially more accurate than the Hough-based one, and robust to curls, oily scalp, noise-corruption, and overlapping hairs, under various white balance.**

***Index Terms*— Hair counting, scalp diagnosis, hair care diagnosis, hair follicle diagnosis, line segment detection.**

I. Introduction

BIOMEDICAL image processing plays an important role in improving the accuracy of medical and cosmetic applications. An accurate medical image allows a doctor to make a more informed decision regarding the treatment of his patient. The image processing technology substantially improves the fields of health and medicine. For example, when investigating hair and scalp conditions are due to living in a different climate zone, age, or gender, image processing technology can be applied in both scalp and skin examinations to provide an accurate diagnosis. Furthermore, household pets are becoming increasingly common in modern society, and pet hair loss is a major issue for many pet owners. Modern image processing technology can also be of benefit in the field of veterinary medicine. The advances in digital image processing technology allows for computer-aided diagnosis and treatment that is capable of dealing with computed tomography (CT), positron emission tomography (PET), cardiovascular, ultrasound, and X-ray images.

Manuscript received September 4, 2014; revised December 3, 2014; accepted December 3, 2014. Date of publication December 18, 2014; date of current version May 4, 2015. This work was supported by the Ministry of Science and Technology of Taiwan under Grant MOST103-2221-E-155-027-MY2 and Grant NSC102-2221-E-155-037-MY2. The associate editor coordinating the review of this paper and approving it for publication was Dr. Anna G. Mignani.

The author is with the Human-Computer Interaction Multimedia Laboratory, Innovation Center for Big Data and Digital Convergence, Department of Electrical Engineering, Yuan Ze University, Zhongli 320, Taiwan (e-mail: hcshih@saturn.yzu.edu.tw).

Color versions of one or more of the figures in this paper are available online at http://ieeexplore.ieee.org.

Digital Object Identifier 10.1109/JSEN.2014.2381363

A. Related Work

Most research topics for hair image processing usually focus on hair modeling, creating a synthesis, and an animated global view. For instance, Mao et al. [1] presented a method for generating a realistic human hair texture. Chen and Zhu [2] proposed a generative model for synthesizing realistic hair images from a stylistic drawing or sketch. It is based on the global hair style regardless of the congenital hair flow for the purpose of hair editing and hair rendering. Yacoob and Davis [3] developed computational models for measuring hair appearance using a multidimensional representation for human identification and hairstyle retrieval. An example-based hair geometry synthesis appeared in [4]. For hair shape modeling, Wang et al. [5] presented a part-based model that was robust to both hair shape and variations in the environment. The so-called subspace clustering dependency guarantees a reasonable output and allows for evaluating the effectiveness of part-wise constraints in an information-theoretic way. In recent years, a number of articles on hair-region segmentation and modeling appeared [6]–[8].

Regarding fine hair, medical image analyses have been focused mainly on pigmented skin lesion images for hair removal [9]–[11] and border detection [12]–[14]. Research literature has been focused mainly on hair segmentation and removal because the hairs are an obstacle for the clinical diagnosis of the scalp. Huang et al. [15] evaluated a hair removal software, DullRazor [16], and proposed conventional matched filters to enhance the curvilinear structures and improve the detection of thin hairs and hairs in shadow. The authors also demonstrated that missing hair intersections can be recovered by applying regional growing algorithms with a color-similarity criteria. However, these aforementioned techniques do not take into consideration the condition of the hairs such as their health condition, density, diameter, oiliness, nor the number of hairs on each single follicle.

Line segments are fundamental component for the analysis of hairs. The Hough transform (HT) [20], [21] is the most popular method to detect lines in images. A very recent survey can be found in [25]. The principle of the HT is based on the scatter position points of an image for identifying the parameters of a certain shape (e.g. straight line or circle). The well-known advantage of the HT is its tolerance for the discontinued line segment and the additive noise. However, since the global voting schemes in the HT do not take line connectivity into account, the HT-based methods do not deal well with cluttered images. Guerreiro *et al.* [26] proposed a so-called STRAGITH method to solve this problem by incorporating connectivity in the voting process. In addition, an improved voting scheme for

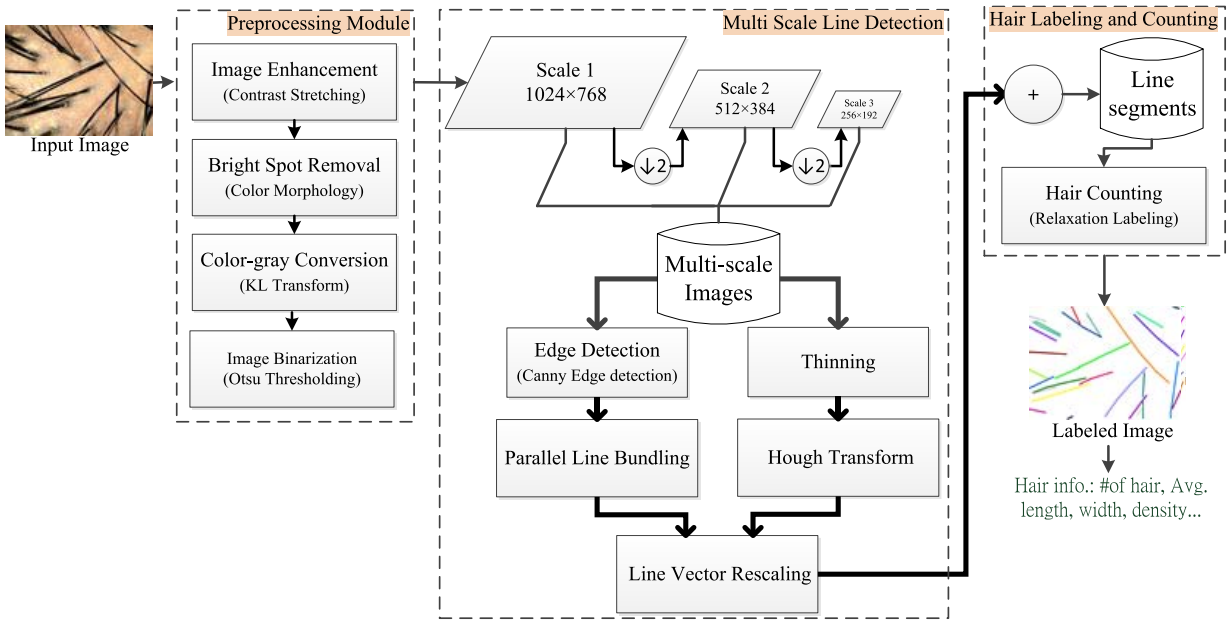

Fig. 1. System flowchart.

the HT that allows a real-time performance even on relatively large images has been developed in [27]. On the other hand, Guru *et al.* [28] presented a line detection algorithm based on small eigenvalue. Similarly, Lee *et al.* [29] proposed a method based on principal component analysis (PCA) to detect straight lines and their orientations. Until now, much of attention in the robust detection of line segments are still challenging and remaining an open frontier [30]–[33].

At present, the diagnosis of a person's hair and scalp relies mainly on the skill and knowledge of professional scalp assessors. The density and diameter of a person's hairs usually reflects the health condition of that person's scalp. Hair counting is usually performed manually by a human assessor, often with unreliable results. In addition, manual counting cannot tell us the diameter, length, and oiliness of the hairs. An automated system capable of counting body hairs was proposed in [17]. In the present study we focused on hair counting on the scalp. Performing a detailed scalp assessment is very time consuming. In an attempt to solve this problem, this study proposed an automated scalp diagnosis system to reduce the time required for making a detailed scalp assessment. Testing images were obtained by means of digital microscopy and then used to, together with the knowledge of professional scalp assessors and doctors, accurately diagnose the hair condition and determine the optimal scalp treatment. Rather than manually counting the hairs on a person's scalp, the proposed system determines the density, diameter, length and level of oiliness of the hairs.

The remainder of this paper is organized as follows. Section II presents the system overview. Section III describes the preprocessing procedures. Section IV presents the multi-scale line detection algorithm. A robust hair labeling and counting approach is illustrated in Section V and the results are discussed in Section VI. Finally, we draw our conclusions in Section VII.

II. System Overview

Fig. 1 illustrates the flow diagram of the proposed system, which includes three stages. In the preprocessing stage, the contrast-stretching method [34] is used to increase the contrast between scalp and hair pixels. To reduce the effect of bright spots, we proposed a robust morphological algorithm for color to smooth out the color and preserve the fidelity of the hair. In addition, we applied the Karhunen-Loève transform (KLT) [24] for each color component and retained the component with the highest energy, and Otsu thresholding [19] to obtain a reliable binary image. In the multi-scale line detection stage we employed a modified Hough transform algorithm to detect the different hair lengths and to reduce any false detection due to noise. Our proposed system enables us to look at curved hairs as multiple pieces of straight lines. To avoid missing hairs when the thinning process is applied, we used edge information to discover any hidden or overlapping hairs. Finally, in the hair labeling and counting stage we employed the relaxation labeling method to label a group of line segments into a meaningful "hair".

III. Preprocessing

Generally speaking, most noise in a test image could be effectively depressed. However, a few discrepancies could not be fully eliminated using the fundamental image processing algorithms. For instance, hairs with a gap in their length suffer from oily spot reflection. When using the conventional region growing method, it will produce many false mergers between individual hairs. To solve this "gap" problem, we present a morphology-based bright spot removal procedure.

A. Data Collection Protocol

The only assumption made in this study is that the hair color is darker than the color of the skin. To simplify the system,

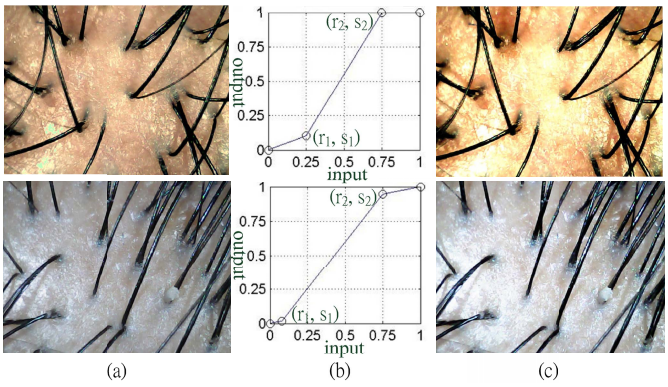

Fig. 2. Image enhancement for the datasets #1 and #2: (a) original image; (b) transformation functions; and (c) contrast stretching image.

we used black and brown hairs for the test images. It should be noted however that the outcome for hairs with other colors will be the same as long as the eye can make the distinction between the color of the hair and the scalp. Hair images are captured from the digital microscope camera (DMC), which enhanced by the built-in LEDs automatically to maintain a stable luminance. We apply a zoom magnification of 85× to capture images. Normally, the images are captured with a resolution of 1024×768 and the equivalent area of scalp is 0.25×0.19 inch^2. In addition, we categorized the captured images into two sets based on the white balance of the DMC. The images with daylight were classified as dataset #1, and those with fluorescent light were classified as dataset #2.

B. Image Enhancement Using Contrast Stretching

In images for hair counting, contrast between hair and scalp pixels is the main factor for determining the quality of the image. However, images often lack sufficient contrast due to the variations in the environment. To solve this problem, color transformation by means of piecewise linear contrast stretching [34] is used to enhance the image. This process expands the dynamic range of the intensity levels allowing it to span the color distance between hair and scalp. Generally speaking, the color distribution of the test image forms bimodal, with the higher-intensity levels denoting the scalp pixels and the lower-intensity levels denoting the hair pixels. In addition, we wanted to increase the color distinction between hair and scalp pixels. We therefore stretched the middle-intensity level, and kept the levels of the low-intensity and high-intensity so as to prevent creating false colors. Fig. 2(b) shows the transformation function for two test datasets and the corresponding results. The two transit points $\{(r_1, s_1), (r_2, s_2)\}$ are empirically assigned The contrast stretching is performed without changing the original hair pixels and without exaggerating the oily-bright pixels. In this study, the transit points $\{(0.25, 0.1), (0.75, 1)\}$ were adopted for dataset #1, whereas $\{(0.08, 0.02), (0.75, 0.85)\}$ were used for dataset #2. As a result, the intensity of the scalp pixels was reduced and the color distinction between scalp and hair was increased. In addition, the pixels of the bright spots remained unchanged, but they were toned down by the bright spot removal process proposed in this study.

C. Bright Spot Removal (BSR)

In the image acquisition step, the oily and moist hair produces bright spots in the middle portions of the hair. The reason for the appearance of these oily spots is due to the light reflecting from the built-in LEDs of the DMC. The surfaces of the moist hair and the oily scalp reflect the supplementary light into the CMOS/CCD sensors of the DMC. This not only results in early sensing saturation, but also replaces the original color with a white spot. Thus we need to eliminate any bright spots prior to counting the hairs, and avoid the situation of "breaks" in the hairs. Unfortunately, it is impossible to precisely know the locations of all hair pixels before the hair is detected. To preserve the scalp information such as the intrinsic color pattern and skin texture for further applications, we utilized color morphological processing approach rather than the binary or gray-scale one for handling this kind of defect.

There are many spatial filtering operators that can suppress the white spots. By treating a white spot as a salt and pepper noise (i.e., impulse noise), we can apply a nonlinear median filter to eliminate it. However, the size of the filtering mask is critical. Another approach is the spatial smooth filter, which can successfully reduce the intensity of the white spot. The drawback however is that the non-hair regions of the test image will also be blurred. To solve these difficulties we used the color-based mathematical morphology (MM) method, and used it as an ordering process. The MM defines the correlation between pixels in the spatial structure, and compares the order. This however requires the ordering and analysis of multi-dimensions. In addition, a Red-Green-Blue (RGB) color image does not have a definite ordering pattern when compared to a gray scale image. Common sequential ordering can be classified into four categories [18] including Marginal-ordering (M-ordering), Conditional-ordering (C-ordering), Partial-ordering (P-ordering), and Reduced-ordering (R-ordering). Each ordering approach has its pros and cons. For instance, M-ordering is quick and simple but it is error prone when it comes to color accuracy, R-ordering decreases computation time, but it lacks integrity, and while C-ordering completely avoids the ambiguous situations caused by the sequential comparison error, it has a high computational complexity.

M-ordering is a compromise approach, based on the component of an individual color vector, without taking the correlation between components into consideration. This will induce a false color that does not exist in the original image. The C-ordering method is based on a specific for comparing the component of a feature vector. The most common method is the so-called lexicographic ordering, which sets priorities between changes, and step-by-step compares the order of each component. Therefore, we present a hybrid ordering approach based on the M-ordering and C-ordering methods that will solve this problem.

Based on our observations, the closing operator in color-based MM brightens low-intensity pixels, while the opening operator darkens high-intensity pixels. We therefore adopted the MM opening operator to depress the bright spot in the middle of the hairs. The opening operator first erodes the image and then dilates it, which is mainly used to eliminate

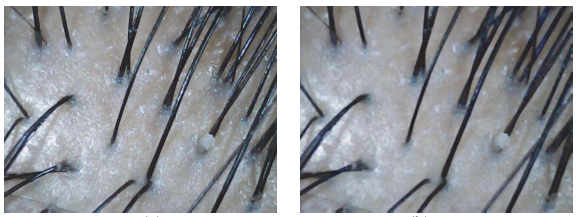

Fig. 3. Oily bright spot removal: (a) original image and (b) result of the bright spot removal.

small structural elements within an image, and it is referenced from the closest peak RGB pixel. The opening operation of image f can be expressed by:

$$\gamma_{\mathrm{M,nB}}(\mathrm{f}) = \tau_{\mathrm{M,nB}}(\varepsilon_{\mathrm{M,nB}}(\mathrm{f})), \tag{1}$$

where $\varepsilon_{\mathrm{M,nB}}$ and $\tau_{\mathrm{M,nB}}$ denote the morphological erosion and dilation of image f of size n by structural element B, respectively, formed by the following formula through pixel x:

$$\varepsilon_{\mathrm{M,nB}}(\mathrm{f})(\mathrm{x}) = \{\mathrm{f}(\mathrm{y}) : \mathrm{f}(\mathrm{y}) = \wedge_{\mathrm{M}}[\mathrm{f}(\mathrm{z})], \mathrm{z} \in \mathrm{n}(Bx)\}, \tag{2}$$

$$\tau_{\mathrm{M,nB}}(\mathrm{f})(\mathrm{x}) = \{\mathrm{f}(\mathrm{y}) : \mathrm{f}(\mathrm{y}) = \vee_{\mathrm{M}}[\mathrm{f}(\mathrm{z})], \mathrm{z} \in \mathrm{n}(Bx)\}, \tag{3}$$

where $\wedge_{\mathrm{M}}$ and $\vee_{\mathrm{M}}$ represent the infimum and supremum in M-ordering respectively. Fig. 3 shows the result of the oily bright spot removal.

In this study we used the KLT to convert the color image to a gray-scale image, with each color component keeping the highest energy component. In the image binarization step, we used Otsu thresholding [19] (referring to the energy of the brightness) in order to obtain a reliable binary image. This process not only increases the process efficiency, but also purifies the resulting image. Fig. 4 compares the line detection if the BSR operation is used, and shows the obvious impact in the binarization and thinning operations. The binarized image with BSR has a reduced bright spot reflection, and in the thinning image the bright spots are transformed into small circles Fig. 4(f) shows that in the line detection phase, the image produced using BSR has less unexpected line segments.

IV. Multi-Scale Line Detection (MSLD)

As aforementioned, the Hough Transform (HT) is one of the most used frameworks for line detection. However, a large amount of hair segments can be lost when the conventional single-scale HT is applied. At the same time, having to choose local maximal values in parametric space is an annoying problem. It is difficult to achieve a convincing result for hair detection because some hairs curl, cross over each other, and there may be dandruff and dust present. First, we propose a multi-scale framework to improve the accuracy of hair detection. Because the parameters of the HT are sensitive to the length of a line segment, we employed three scales of the images to the HT, while preserving the different lengths of the hairs. In addition, we applied a parallel line bundling (PLB) algorithm to restore any hidden or overlapped hairs. Finally, the vectorized line segments are used as input data for the hair labeling and counting module.

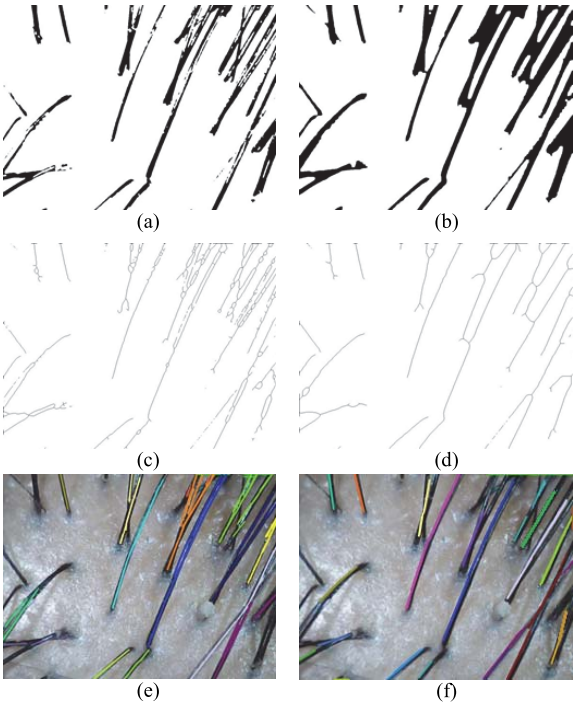

Fig. 4. Comparisons of the hair thinning and line detection. (a) Binarized image without BSR (b) binarized image with BSR, (c) thinning image without BSR, (d) thinning image with BSR, (e) line detection without BSR, and (f) line detection with BSR.

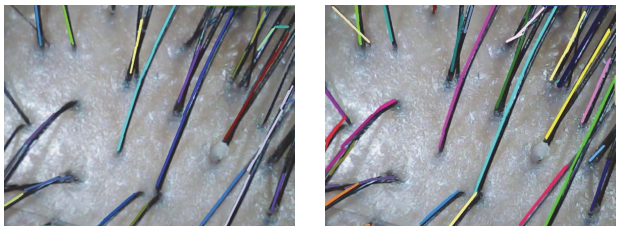

Fig. 5. Comparison of the single scale and multi-scale line detection: (a) result image using single scale method and (b) result image using multi-scale method.

In this study, three scales of images are applied for the HT including 1024×768 (original scale), 512×384, and 256×192. Two processing methods are applied to the scaled images, the edge detection and the thinning process. The proposed PLB algorithm is applied to the edge image to discover the missing line segments, and the HT is applied to the thinning images to extract the line segments. By taking advantage of the PLB algorithm, the hidden and overlapping hairs can be restored. Finally, the vectorized line segments are rescaled into their original size of 1024×768, and integrated by a logical OR operator. As shown in Fig. 5, the use of a single-scale HT does not allow all hairs to be detected due to the variations in length and curliness of the hairs. Fig. 5(a) shows that when a hair appears in near-parallel, overlaps with other hairs, or if the curvature of the hair exceeds the tolerance of the HT, then we end up with a large amount of hairs that are missed and a lot of line segments that are mislabeled. Fig. 5(b) shows the result using the line segments from all the scales, thereby improving the insufficiency of the single scale.

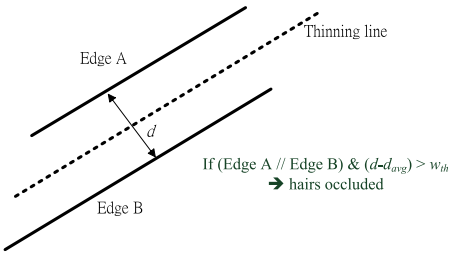

Fig. 6. Thinning line sandwiched by two parallel lines with the distance d.

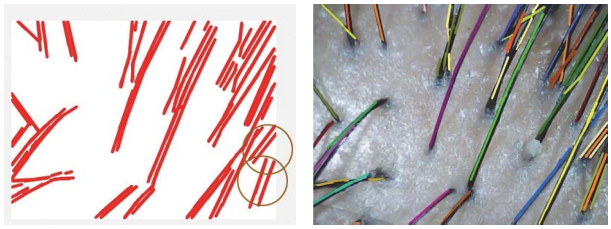

Fig. 7. Result of PLB algorithm: (a) edge map and (b) the restored image. The circled position shows that the hidden hairs can be discovered.

A. Parallel Line Bundling (PLB)

In the image binarization step, the scalp pixels located between two hairs are labeled as part of a hair, due to the incorrectly assumed connection of two individual hairs. Moreover, when two hairs are too close together or overlap each other, one or both hairs will be missed if the thinning algorithm is applied directly. Therefore, we used edge information to discover any hidden or overlapping hairs. From the edge viewpoint, two parallel edges can be extracted from a hidden hair or multiple hairs that overlap. Based on the distance between two parallel lines, we can determine if there are any hairs that are hidden or are overlapping. First, we apply the Canny edge detector [22] to obtain the edge map. As shown in Fig. 6, suppose that two parallel lines A and B are detected expressed by $ax + by + c_{\mathrm{a}} = 0$ and $ax + by + c_{\mathrm{b}} = 0$, where d denotes the distance between edge lines A and B, and where $d = |c_a - c_b| / \sqrt{a^2 + b^2}$. Second, we compute the average distance d_{avg} between the parallel lines that sandwich a thinning line. If the distance value is large than d_{avg}, we will continue discovering hidden hairs, when $(dd_{avg}) > w_{th}$, where w_{th} denotes the bounding factor. This factor will be empirically modified by the resolution of the scalp image. In Fig. 7(a), circles indicate hidden hairs, as shown in Fig. 7(b).

V. Hair Labeling and Counting

Using the MSLD module, we derived a set of line segments. The hairs were realized as a cluster of piecewise line vectors with different lengths depending on the curvature and the orientation of the hair flow. This aim of this study was to accurately count the number of hairs on a scalp. This can be viewed as a clustering and labeling problem. The goal is to assemble a group of line segments into a semantic "hair" and assign a unique label. Because each hair consists of a cluster of mutually correlated line segments, we assigned a unique label to each cluster. We adopted the Relaxation labeling algorithm [23] for the identification of each individual line segment to determine which it line segments it was associated with. Fig. 8(a), shows an example of 10 individual line segments that were labeled as being from the same hair, and were then plotted onto the (ρ, θ)-plane, as shown in Fig. 8(b). The resulting peak value of the accumulated map at the crosspoint is 10.

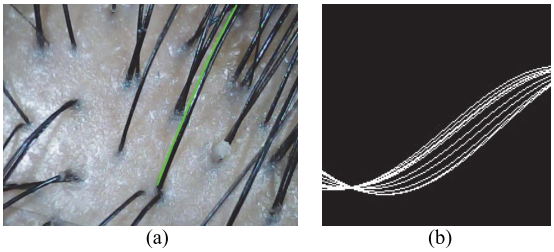

Fig. 8. Example of line segment labeling. (a) Result image. (b) Polar corrdinate system. Green line of the result image corresponds to a labeled hair, which is constructed from ten small line segments. Each line of the segments is mapped onto the polar coordinate system (ρ, θ), and then the crosspoint converts to the image space as a labeled green line.

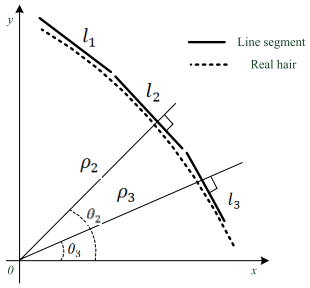

Fig. 9. Conceptual schematics of the labeling algorithm. Determining two individual lines if belongs to the same hair based on corresponding orientation θ and the distance from origin (i.e., ρ).

A. Relaxation Labeling

Relaxation Labeling (RL) is a mutually associative regression method, which uses symbols to describe the shape of model. It aims to match the target object (i.e., line segment in this paper) with the symbol or so-called marker (i.e., hair label). The RL algorithm first assigns a set of random markers. Then, through iterative calculations a more accurate and precise set of markers is obtained. In this study, the RL algorithm is treated as a clustering method for labeling every line segment. A compatibility factor in the RL algorithm provides the clue for converging the grouping operation. Here, the compatibility is in terms of orientation and distance from the origin. As shown in Fig. 9, line segments l_1, l_2, and l_3 should be assigned to the same hair label, based on their orientation and distance values from the origin.

Let C(i, λ, j, λ') denote the compatibility of line segmenti labeled λ with line segment j labeled λ' with the constraint that

$$\sum_{\lambda} \mathrm{C}(\mathrm{i}, \lambda, \mathrm{j}, \lambda') = 1, \quad \text{for } \forall \mathrm{i}, \mathrm{j}, \lambda', \lambda \tag{4}$$

Compatibility C represents the inter-dependency between line segment j labeled as λ' and line segment i labeled as λ. If the compatibility is determined only by the distance from the origin, it may suffer from false interpretation. Therefore, we defined compatibility as follows,

$$C(i,\lambda,j,\lambda') = \begin{cases} -1 & i \notin S_j \\ \varepsilon\left|cos\left[\theta_{\mathrm{i}}(\lambda) - \theta_{\mathrm{j}}(\lambda')\right]\right| + (1-\varepsilon)\frac{\rho_{\mathrm{i}}(\lambda)}{\rho_{\mathrm{j}}(\lambda')} & i \in S_j \cap \lambda \neq \lambda' \\ 0 & otherwise \end{cases} \tag{5}$$

where ε denotes the weighting factor between distance and orientation confidences, S_j denotes the neighboring hypothesis for line segment j, $\theta_{\mathrm{i}}(\lambda)$ denotes the direction from line segment i to line segment j labeled as λ, and $\rho_{\mathrm{i}}(\lambda)$ denotes the distance from the origin between line segment i and line segment j labeled as λ. If $\rho_{\mathrm{j}}(\lambda)$ is high and C(i, λ, j, λ') is positive, then $\rho_{\mathrm{i}}(\lambda)$ increases. This labeling algorithm is an iterative parallel procedure analogous to the label-discarding rule used in probabilistic relaxation. The operator iteratively adjusts the label weights based on the other weights and compatibilities. For each line segment and each label, a new weight $q_i^{(r)}(\lambda)$ is computed as follows

$$q_i^{(r)}(\lambda) = \sum_{j,j\neq i}\sum_{\lambda'} \mathrm{C(i},\lambda,\mathrm{j},\lambda')p_j^{(r)}(\lambda') \tag{6}$$

where $^{\mathrm{r}}$ denotes the r^{th} iteration. In Eq. (6), the product sum is the expectation that line segment i has been labeled λ, given the evidence provided by line segment j. Thus, $q_i^{(r)}(\lambda)$ is a weighted sum of current assignment values $p_i^{(r)}(\lambda)$. A new assignment can be updated using

$$p_i^{(r+1)}(\lambda) = \frac{p_i^{(r)}(\lambda)\left[1+q_i^{(r)}(\lambda)\right]}{\sum_{j=1}^{m} p_i^{(r)}(\lambda')\left[1+q_i^{(r)}(\lambda')\right]} \tag{7}$$

Here, we simply pick $p_i^{(r)}(\lambda)$ and $C(i,\lambda,j,\lambda')$ and apply Eq. (7) to recursively update $p_i^r(\lambda)$ until they stop varying or converge to 1. Each line segment is iteratively verified until it has been assigned to the correct semantic label "hair".

VI. Experimental Results

To evaluate our system, we captured 40 scale images with a resolution of 1024×768 from the UPMOST (UPG622) DMC as the dataset for testing. According to the white balance of the DMC, we classified test images into two groups, which are dataset #1 and dataset #2.

A. Experiment 1: Cross-Validation of the Line Detection

Fig. 1 (b)-(d) shows the results of the preprocessing module, including the bright spot removal (BSR), binarization, and thinning processes. In order to evaluate the performance of the multi-scale line detection algorithm, the testing images we applied three different scales for the HT for extracting line segments. The hair labeling mechanism was then used to determine the number of the hairs. As shown in Fig. 10 (e)-(f), the colored lines represent the label of the hair. In other words hairs can be labeled accurately even when they are crossed or overlapped. The following section demonstrates the objective measurement of hair counting regarding precision and recall rates. We compared four cases using combinations of the BSR and MSLD modules, including BSR + MSLD, without both BSR and MSLD, BSR-only, and MSLD-only.

TABLE I
Comparison of the System Sensitivity for the Module Usages in the Line Detection

Dataset	Module Usages	Precision	Recall
#1	**Without** BSR & MSLD	92.77%	74.79%
	With BSR **only**	93.04%	80.67%
	With MSLD **only**	93.20%	77.42%
	With BSR & MSLD	**94.98%**	**83.50%**
#2	**Without** BSR & MSLD	96.52%	75.14%
	With BSR **only**	97.09%	78.43%
	With MSLD **only**	95.95%	77.93%
	With BSR & MSLD	**98.05%**	**85.56%**

TABLE II
System Performance for With/Without PLB

Dataset	With/without PLB	Precision	Recall
#1	**Only** with BSR & MSLD	94.98%	83.50%
	With PLB	**95.25%**	**88.59%**
#2	**Only** with BSR & MSLD	98.05%	85.56%
	With PLB	**98.53%**	**89.12%**

Table I compares system sensitivity based on module usage. We proposed the morphology-based BSR and MSLD mechanisms for improving the performance of hair detection, obtaining rates of precision of 94.98% and 98.05% respectively. Compared with the conventional HT line detection method this was an improvement of 2% and 1.5% for dataset #1 and dataset #2 respectively. From a recall rate point of view it was also higher than other module combinations. On average, we achieved a 9% and 10% recall rate. Based on our observations after applying BSR the precision rate was boosted. However, when the MSLD was applied to dataset #2, the precision rate decreased, because it created great amounts of light reflections in the oily scalp region. Similarly, the bright spot in the middle of the hair was seriously enhanced, resulting in the lowering of the precision rate.

B. Experiment 2: System Refinement Using the PLB Algorithm

Table II shows the efficiency of the PLB algorithm. Our proposed PLB method enabled the system to extract the missing hairs, with a 0.5% improvement in the precision rate, and a 5% improvement in the recall rate. The PLB algorithm can serve as a system fine-tuning process, increasing the system performance to 96.89% on average. This is reasonable because hidden hairs are not a frequent occurrence. In addition, we can control the resolution and the angle of the hair images from the microscope to avoid this situation.

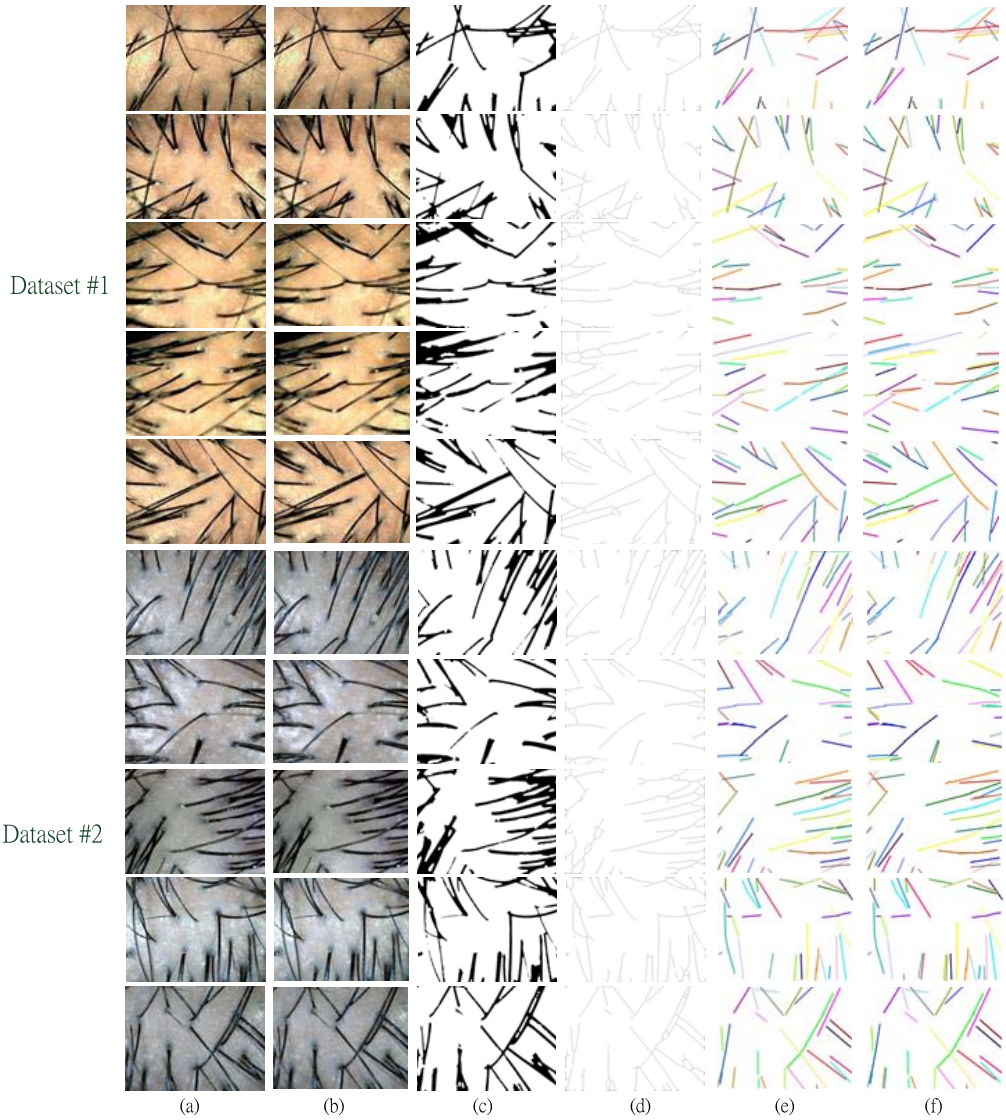

Fig. 10. Result images for line detection. (a) The original images, (b) BSR result images, (c) binarized images with BSR, (d) thinning images with BSR, (e) result images using BSR and MSLD, and (f) result images by applying PLB algorithm to (e).

TABLE III
TIME OCCUPANCY OF EACH MODULE COMPARED WITH TOTAL EXECUTION

	Pre-processing	MSLD	Thinning	Hair labeling and counting	PLB
Time occupancy	8.95%	29.18%	20.71%	25.27%	15.89%

C. Experiment 3: Complexity Analysis

When it comes to system complexity analysis, we are aware that the proposed hair counting system is more time consuming. On average, a high-resolution test image required less than 4 sec to derive the hair count information. Table III illustrates the time required for each module in comparison with the total execution time. The MSLD uses three scales to obtain a set of line segments, which required most of the execution time. The process of the HT projecting the edge map onto the (ρ, θ) space to extract the local maximum is time-intensive. In order to overcome this problem, we used only two scales in MSLD. However, this attempt resulted in a bad performance. In addition, the thinning process occupied more than a quarter of the total processing time. It is a trade-off between execution time and system accuracy.

VII. CONCLUSION

This study presented an automate hair segmentation and counting system to reduce the time required for making a detailed scalp assessment by human assessors. First, oily and moist hairs tend to generate a bright spot in the middle of the hair. Before counting the number of hairs, we need to eliminate this bright spot on the hairs so as to avoid the problem of double-counting some hairs. Second, the wavy and curly hairs tend to result in line detection faults. When a hair is not straight, the conventional line detection algorithm is invalid. Third, under-estimation of the number of hairs

occurs when hairs cross and occlude each other, making it very difficult to locate all hairs accurately. Finally, because the scalp is comparatively unexposed, the image of the scalp is often blurred or difficult to see. In addition the scalp is often insufficiently illuminated or over-exposed. The framework of this paper can be seen as the first step towards intelligent computer-aided medical image processing for cosmetic hair and scalp treatment applications.

ACKNOWLEDGMENT

The author would like to thank B.-S. Lin to develop the program implementation initially and test the hair samples, and E. Chen and M. Chien from Macrohi LTD., Taiwan, for providing technical consultant.

REFERENCES

[1] X. Mao, M. Kikukawa, K. Kashio, and A. Imamiya, "Automatic generation of hair texture with line integral convolution," in *Proc. IEEE Int. Conf. Inf. Vis.*, Jul. 2000, pp. 303–308.

[2] H. Chen and S.-C. Zhu, "A generative sketch model for human hair analysis and synthesis," *IEEE Trans. Pattern Anal. Mach. Intell.*, vol. 28, no. 7, pp. 1025–1040, Jul. 2006.

[3] Y. Yacoob and L. S. Davis, "Detection and analysis of hair," *IEEE Trans. Pattern Anal. Mach. Intell.*, vol. 28, no. 7, pp. 1164–1169, Jul. 2006.

[4] L. Wang, Y. Yu, K. Zhou, and B. Guo, "Example-based hair geometry synthesis," in *Proc. ACM SIGGRAPH*, Aug. 2009, Art. ID 56.

[5] N. Wang, H. Ai, and F. Tang, "What are good parts for hair shape modeling?" in *Proc. IEEE Conf. Comput. Vis. Pattern Recognit. (CVPR)*, Providence, RI, USA, Jun. 2012, pp. 662–669.

[6] P. Julian, C. Dehais, F. Lauze, V. Charvillat, A. Bartoli, and A. Choukroun, "Automatic hair detection in the wild," in *Proc. 20th IEEE ICPR*, Aug. 2010, pp. 4617–4620.

[7] D. Wang, S. Shan, H. Zhang, W. Zeng, and X. Chen, "Isomorphic manifold inference for hair segmentation," in *Proc. 10th IEEE Automat. Face Gesture Recognit. (FG)*, Apr. 2013, pp. 1–6.

[8] C. Rousset and P. Y. Coulon, "Frequential and color analysis for hair mask segmentation," in *Proc. 15th IEEE ICIP*, San Diego, CA, USA, Oct. 2008, pp. 2276–2279.

[9] O. Debeir, C. Decaestecker, J. L. Pasteels, I. Salmon, R. Kiss, and P. Van Ham, "Computer-assisted analysis of epiluminescence microscopy images of pigmented skin lesions," *Cytometry*, vol. 37, no. 4, pp. 255–266, 1999.

[10] P. Schmid-Saugeon, J. Guillod, and J.-P. Thiran, "Towards a computer-aided diagnosis system for pigmented skin lesions," *Comput. Med. Imag. Graph.*, vol. 27, no. 1, pp. 65–78, 2003.

[11] N. H. Nguyen, T. K. Lee, and M. S. Atkins, "Segmentation of light and dark hair in dermoscopic images: A hybrid approach using a universal kernel," *Proc. SPIE, Med. Imag.*, vol. 7623, pp. 76234N-1–76234N-8, Mar. 2010.

[12] M. E. Celebi *et al.*, "Border detection in dermoscopy images using statistical region merging," *Skin Res. Technol.*, vol. 14, no. 3, pp. 347–353, 2008.

[13] M. E. Celebi, H. Iyatomi, G. Schaefer, and W. V. Stoecker, "Lesion border detection in dermoscopy images," *Comput. Med. Imag. Graph.*, vol. 33, no. 2, pp. 148–153, 2009.

[14] T. Donadey *et al.*, "Boundary detection of black skin tumors using an adaptive radial-based approach," *Proc. SPIE, Med. Imag.*, vol. 3979, pp. 810–816, Jun. 2000.

[15] A. Huang, S.-Y. Kwan, W.-Y. Chang, M.-Y. Liu, M.-H. Chi, and G.-S. Chen, "A robust hair segmentation and removal approach for clinical images of skin lesions," in *Proc. 35th Annu. Int. Conf. IEEE EMBS*, Osaka, Japan, Jul. 2013, pp. 3315–3318.

[16] T. Lee, V. Ng, R. Gallagher, A. Coldman, and D. McLean, "Dullrazor: A software approach to hair removal from images," *Comput. Biol. Med.*, vol. 27, no. 6, pp. 533–543, 1997. [Online]. Available: http://www.dermweb.com/dull_razor/

[17] R. Hoffmann, "TrichoScan. A new instrument for digital hair analysis," *Hautarzt*, vol. 53, no. 12, pp. 798–804, 2002.

[18] H.-C. Shih and E.-R. Liu, "Adaptive region merging approach for morphological color image segmentation," in *Proc. Asian Conf. Comput. Vis. (ACCV)*, Singapore, 2014.

[19] N. Otsu, "A threshold selection method from gray-level histograms," *IEEE Trans. Syst., Man, Cybern.*, vol. 9, no. 1, pp. 62–66, Jan. 1979.

[20] P. V. C. Hough, "Method and means for recognizing complex patterns," U.S. Patent 3 069 654, Dec. 18, 1962.

[21] R. O. Duda and R. E. Hart, "Use of the Hough transformation to detect lines and curves in pictures," *Commun. ACM*, vol. 15, no. 1, pp. 11–15, Jan. 1972.

[22] J. Canny, "A computational approach to edge detection," *IEEE Trans. Pattern Anal. Mach. Intell.*, vol. PAMI-8, no. 6, pp. 679–698, Nov. 1986.

[23] A. Rosenfeld, R. A. Hummel, and S. W. Zucker, "Scene labeling by relaxation operations," *IEEE Trans. Syst., Man, Cybern.*, vol. SMC-6, no. 6, pp. 420–433, Jun. 1976.

[24] K. R. Rao and P. C. Yip, *The Transform and Data Compression Handbook*. Boca Raton, FL, USA: CRC Press, 2000.

[25] P. Mukhopadhyay and B. B. Chaudhuri, "A survey of Hough transform," *Pattern Recognit.*, vol. 48, no. 3, pp. 993–1010, 2015.

[26] R. F. C. Guerreiro and P. M. Q. Aguiar, "Connectivity-enforcing Hough transform for the robust extraction of line segments," *IEEE Trans. Image Process.*, vol. 21, no. 12, pp. 4819–4829, Dec. 2012.

[27] L. A. F. Fernandes and M. M. Oliveira, "Real-time line detection through an improved Hough transform voting scheme," *Pattern Recognit.*, vol. 41, no. 1, pp. 299–314, 2008.

[28] D. S. Guru, B. H. Shekar, and P. Nagabhushan, "A simple and robust line detection algorithm based on small eigenvalue analysis," *Pattern Recognit. Lett.*, vol. 25, no. 1, pp. 1–13, 2004.

[29] Y.-S. Lee, H.-S. Koo, and C.-S. Jeong, "A straight line detection using principal component analysis," *Pattern Recognit. Lett.*, vol. 27, no. 14, pp. 1744–1754, 2006.

[30] R. G. von Gioi, J. Jakubowicz, J.-M. Morel, and G. Randall, "LSD: A fast line segment detector with a false detection control," *IEEE Trans. Pattern Anal. Mach. Intell.*, vol. 32, no. 4, pp. 722–732, Apr. 2010.

[31] S. Du, C. Tu, B. J. van Wyk, and Z. Chen, "Collinear segment detection using HT neighborhoods," *IEEE Trans. Image Process.*, vol. 20, no. 12, pp. 3612–3620, Dec. 2011.

[32] R. F. C. Guerreiro and P. M. Q. Aguiar, "Extraction of line segments in cluttered images via multiscale edges," in *Proc. 20th IEEE ICIP*, Sep. 2013, pp. 3045–3048.

[33] A. Borkar, M. Hayes, and M. T. Smith, "Polar randomized Hough transform for lane detection using loose constraints of parallel lines," in *Proc. IEEE ICASSP*, May 2011 pp. 1037–1040.

[34] R. C. Gonzalez and R. E. Woods, *Digital Image Processing*, 3rd ed. Reading, MA, USA: Addison-Wesley, 2008.

[35] H. C. Shih and B. S. Lin, "Hair segmentation and counting algorithms in microscopy image," in *Proc. IEEE ICCE*, Las Vegas, NV, USA, Jan. 2014.

Huang-Chia Shih (M'08) received the B.S. (Hons.) degree in electronic engineering from the National Taipei University of Technology, Taipei, Taiwan, in 2000, and the M.S. and Ph.D. degrees in electrical engineering from National Tsing Hua University, Hsinchu, Taiwan, in 2002 and 2008, respectively.

He has been an Assistant Professor with the Department of Electrical Engineering, Yuan Ze University, Zhongli, Taiwan, since 2010. His research interests are content-based multimedia processing, pattern recognition, and human-computer interaction. He served as a Visiting Scholar with the Department of Electrical Engineering, University of Washington, Seattle, WA, USA, from 2006 to 2007, and a Visiting Professor with the John von Neumann Faculty of Informatics, Obuda University, Budapest, Hungary, in 2011. He received the Young Researcher Award from Yuan Ze University in 2014, the Kwoh-Ting Li Young Researcher Award from ACM Taipei/Taiwan Chapter in 2014, the Pan Wen Yuan Exploration Research Award from the Pan Wen Foundation in 2013, the Best Paper Award of the 2013 IEEE International Symposium on Consumer Electronics from the IEEE Consumer Electronics Society, the Project of Outstanding Junior Research Investigators (two years) from the National Science Council of Taiwan in 2012, and the Best Doctoral Dissertation from the Image Processing and Pattern Recognition Society, Taiwan, in 2009.

Dr. Shih has published over 40 technical papers in refereed journals and conference proceedings and served as a Program Committee Member and reviewer for international journals and conferences.